Photo-/Electroinduced Irreversible Isomerization of 2,2'-Azobispyridine Ligands in Arene Ruthenium(II) Complexes

Jonathan Long, Divyaratan Kumar, Claire Deo, Pascal Retailleau, Galina V Dubacheva, Guy Royal, Juan Xie, Nicolas Bogliotti

Photo/Electro-Induced Irreversible Isomerization of 2,2'-Azobispyridine Ligand in Arene Ruthenium(II) Complexes

Jonathan Long,[a] Divyaratan Kumar,[a] Claire Deo,[a] Pascal Retailleau,[b] Galina V. Dubacheva,[a,c] Guy Royal,[c] Juan Xie,[a] and Nicolas Bogliotti*[a]

Dedication ((optional))

[a] J. Long, D. Kumar, C. Deo, Dr. G. Dubacheva, Prof. J. Xie, Dr. N. Bogliotti
Université Paris-Saclay, ENS Paris-Saclay, CNRS, Photophysique et Photochimie Supramoléculaires et Macromoléculaires
91190, Gif-sur-Yvette, France
E-mail: nicolas.bogliotti@ens-paris-saclay.fr
[b] Dr. P. Retailleau
Université Paris-Saclay, CNRS, Institut de Chimie des Substances Naturelles, UPR 2301
91198, Gif-sur-Yvette, France
[c] Dr. G. V. Dubacheva, Prof. G. Royal
Université Grenoble Alpes, CNRS, Département de Chimie Moléculaire (UMR5250)
F38400, Grenoble, France

Supporting information for this article is given via a link at the end of the document.

Abstract: Novel arene Ru(II) complexes containing 2,2'-azobispyridine ligands were synthesized and characterized using ^{1}H- and ^{13}C-NMR, UV/Vis spectroscopy, electrochemistry, DFT calculations and single crystal X-ray diffraction. *Z*-configured complexes featuring unprecedented 7-membered chelate ring involving the nitrogen atom of both pyridines were isolated and were shown to undergo irreversible isomerization to the corresponding *E*-configured 5-membered chelate complexes in response to light or electrochemical stimulus.

Introduction

Azopyridine is a photochromic organic compound that undergoes reversible *E*–*Z* isomerization upon UV irradiation. It is also a well-known ligand for metal center[1], with resulting complexes used as magnetic resonance imaging probes[2], cytotoxic agents against cancer cell,[3,4,5] or as building components in switchable materials.[6,7,8,9,10] The ligand properties of azobispyridine have been investigated towards a number of metals, such as Cd(II)[11,12,13,14,15,16], Cu(II)[13,15,17,18], Re(I)[19,20,21], Cu(I)[13,18,22], Ni(II)[13,15,23], Zn(II)[15,23], Ru(II)[24,25], Ag(I)[26,27], Co(II)[11,13], Re(II) and (V)[21], Pt(II)[28], Hg(II)[15], Au(I)[26], Mn(II)[13], W(0) and Os(0)[29], and Ti(II)[30], giving rise to new types of polymer structures involving π-π and π-p stacking of the ligand[13,14,15,16,30]. The coordination properties to the metal center are obviously impacted by the position of the nitrogen atom in the pyridine ring of the ligand. Linear patterns such as **I** and **II** are most common for 4,4'- and 3-3'-azobispyridine[11-15,18,19,21,23,25,26,29] (Figure 1), while bidentate coordination mode with five-membered chelate rings such as **IIIa**[16,17,20,22,27,28], or more rarely tridentate coordination such as **IIIb,** are found with *E*-2,2'-azobispyridine.[31,32] A peculiar property of the latter ligand in these systems is that it usually does not undergo *E*-*Z* photo-isomerization as a consequence of the geometrical constraints imposed by the strong bonding to the metal center, with one notable exception found in the case of Ag(I) complex.[26] To the best of our knowledge, metal complexes of type **IV** involving coordination of the two nitrogen atoms of the pyridine rings of *Z*-2,2'-azobispyridine, suggested by Baldwin as early as 1969, have never been reported so far.[33]

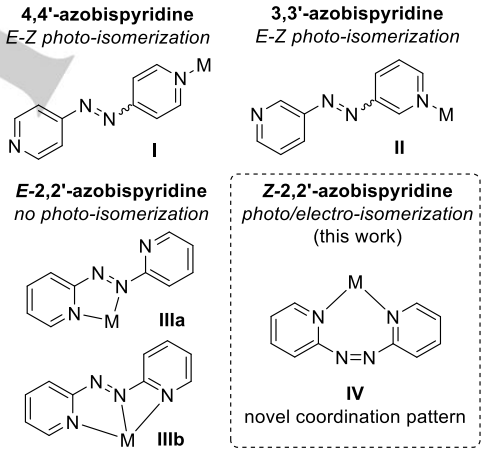

Figure 1. Common coordination pattern exhibited by azobispyridine (**I**, **II**, **III**) and a novel 7-membered chelate ring described in the present study (**IV**).

In this work, we report the synthesis of novel arene ruthenium(II) complexes derived from 2,2'-azobispyridine, notably exhibiting an unprecedented *Z*-configured seven-membered chelate ring with the metal center (Scheme 1). The study of their behavior in response to light or redox stimuli revealed a complete and irreversible *Z*→*E* isomerization with concomitant rearrangement of the coordination pattern of the ligand.

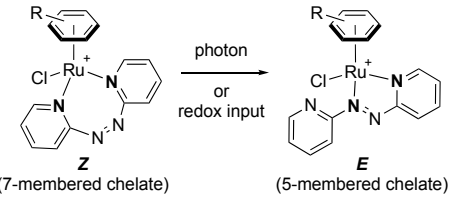

Scheme 1. Photon or redox input-induced isomerization of *Z*-configured 7-membered chelate Ru complexes into *E*-configured 5-membered chelate complexes.

Results and Discussion

Synthesis and molecular structure of *E*-2$^+$, *E*-3$^+$, *E*-4$^+$, *Z*-5$^+$ and *Z*-6$^+$

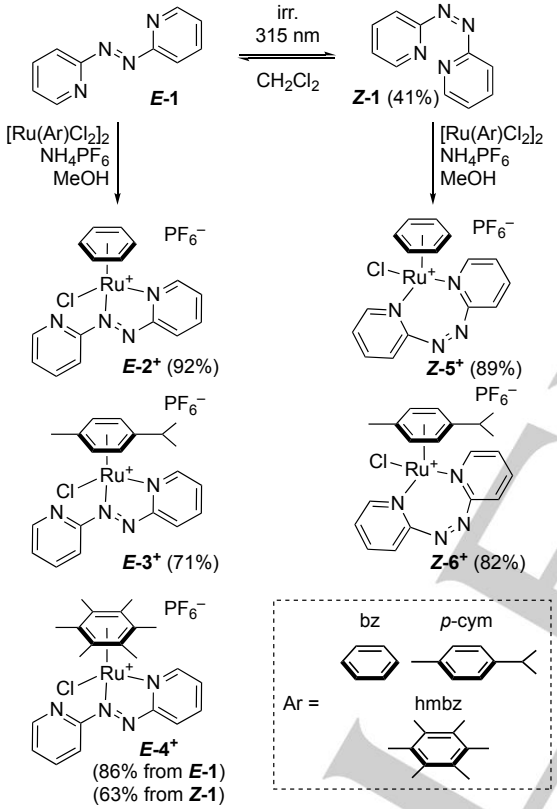

Scheme 2. Synthesis of Ru complexes ***E*-2**$^+$, ***E*-3**$^+$, ***E*-4**$^+$, ***Z*-5**$^+$ and ***Z*-6**$^+$.

Irradiation of a dichloromethane solution of the known azobispyridine ***E*-1**[33,34] at 315 nm (P = 45 mW.cm^{-2}) for 4 h resulted in a *ca.* 6:4 mixture of *E* and Z isomers, which were separated by column chromatography to yield 41% of ***Z*-1**, stable for several months when stored in the dark below 4°C (Scheme 2). Reaction of ***E*-1** in methanol with ruthenium dimers $[Ru(Ar)Cl_2]_2$, where Ar = benzene (bz), *para*-cymene (*p*-cym) or hexamethylbenzene (hmbz), followed by counter-ion exchange with NH_4PF_6 yielded the expected complexes ***E*-2**$^+$, ***E*-3**$^+$[35] and ***E*-4**$^+$ as dark red powders in good yield (71 to 92%, Scheme 2). The identity of these complexes was assessed by ^{1}H- and ^{13}C-NMR spectroscopies, HRMS analysis and X-ray diffraction studies. Besides the expected signals corresponding to arene ligands, the ^{1}H-NMR spectra in dichloromethane-d_2 of all *E* complexes revealed a similar pattern with a set of 8 signals (each integrating for 1H) between 7.5 and 9.5 ppm (see SI), corresponding to the magnetically non-equivalent H atoms of the azobispyridine ligand, in agreement with previous reports.[3] The non-symmetric nature of the azobispyridine ligand in these complexes was also confirmed by ^{13}C-NMR spectroscopy showing eight signals accounting for pyridine CH groups in the range 116–154 ppm. The two quaternary carbons next to nitrogen atoms appeared at 163.0 and 162.4 ppm in ***E*-3**$^+$ (only one visible at 164.4 ppm in ***E*-4**$^+$), while none were observed in the case of ***E*-2**$^+$, presumably due to long relaxation times.

Single crystals of ***E*-3**$^+$ and ***E*-4**$^+$ suitable for X-ray analysis were obtained by chloroform vapor diffusion in an acetone solution (Figure 2). The molecular structure of both complexes exhibits a classical "three-legged piano stool" geometry around Ru center, with Ru–N bond lengths ranging between 1.998 and 2.055 Å, Ru-centroid distances of 1.719 and 1.741 Å, azo N–N bond lengths around 1.27 Å, and N1-Ru-N3 and N1-Ru-Cl angles being around 75° and 84°, respectively (Table 1). These values compare well with those previously reported.[3] The most striking difference between the two complexes is the relative orientation of both pyridine rings, which are almost coplanar in the case of ***E*-3**$^+$ and significantly twisted in the case of ***E*-4**$^+$, as revealed by dihedral angle N1-C2-C1-N4 values of 30.42° and 128.52°, respectively, thereby evidencing the influence of arene ligand substitution on the geometry of the complex.

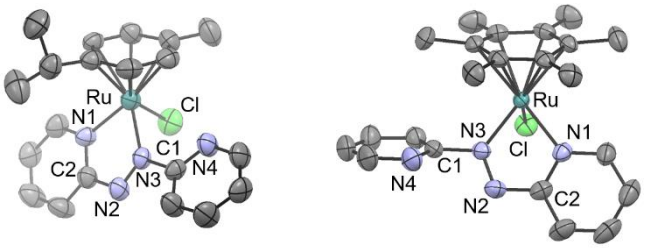

Figure 2. ORTEP representation (thermal ellipsoids drawn at 50% probability level) of ***E*-3**$^+$ (left) and ***E*-4**$^+$ (right) with atom numbering. The hydrogen atoms and PF_6^- anion have been removed for clarity.

Table 1. Selected bond lengths (Å) and angles (deg.) for complexes ***E*-3**$^+$ and ***E*-4**$^+$.

	***E*-3**$^+$	***E*-4**$^+$
Ru-N1	2.035	2.055
Ru-N3	2.046	1.998
N2-N3	1.267	1.274
Ru-cent.[a]	1.719	1.741
N1-Ru-N3	75.15	74.82
N1-Ru-Cl	83.70	84.15
N1-C2-C1-N4	30.42	128.52
N1-Ru-N3-N2	0.82	1.29

[a] cent.=centroid of arene moiety

Reaction of ***Z*-1** with $[Ru(bz)Cl_2]_2$ and $[Ru(p\text{-cym})Cl_2]_2$ in the dark under otherwise the same conditions yielded the dark green and deep yellow complexes ***Z*-5**$^+$ (89%) and ***Z*-6**$^+$ (82%), respectively. The ^{1}H-NMR spectra recorded in dichloromethane-d_2 revealed a significant simplification of the signals as compared to the corresponding *E* isomers, with four peaks between 7.41 and 9.04 ppm each integrating for 2H, ascribed to magnetically equivalent hydrogen atoms of the pyridine rings. The symmetric nature of the azobispyridine ligand in those complexes was also assessed in the ^{13}C-NMR spectra, showing a set of five signals in the range 120–164 ppm. In the solid state, both complexes remained stable for months when stored in the dark at -4°C, and freshly prepared CH_2Cl_2 solutions thereof could be easily handled over the course of several hours if kept at rt away from light (Figure S1,S2).

Surprisingly, treatment of ***Z*-1** with $[Ru(hmbz)Cl_2]_2$ did not lead to the corresponding *Z*-complex but rather to ***E*-4**$^+$ (in 63% yield) as unambiguously determined from ^{1}H and ^{13}C-NMR analysis. Here, it is likely that the *Z*-complex similar to ***Z*-5**$^+$ and ***Z*-6**$^+$ is unstable in solution and rapidly isomerizes to the *E* form because of the steric hindrance of the hmbz ligand.

Despite our efforts, suitable crystals for X-ray analysis of ***Z*-5**$^+$ and ***Z*-6**$^+$ could not be obtained, thereby leading us to investigate the geometry of putative structures using DFT calculations. Our modeling studies revealed that both complexes could exist as two distinct sets of diastereoisomers ***Z*-5**$^+$ / ***Z*-5'**$^+$ and ***Z*-6**$^+$ / ***Z*-6'**$^+$, with N=N linkage facing either the chloro or the arene ligand. Geometry optimization performed at the B3LYP/6-311G(d,p)/LANL2DZ level revealed an increased stability (around 80 kJ/mol) of both ***Z*-5**$^+$ and ***Z*-6**$^+$ as compared to their diastereoisomers ***Z*-5'**$^+$ and ***Z*-6'**$^+$ (Figure 3).

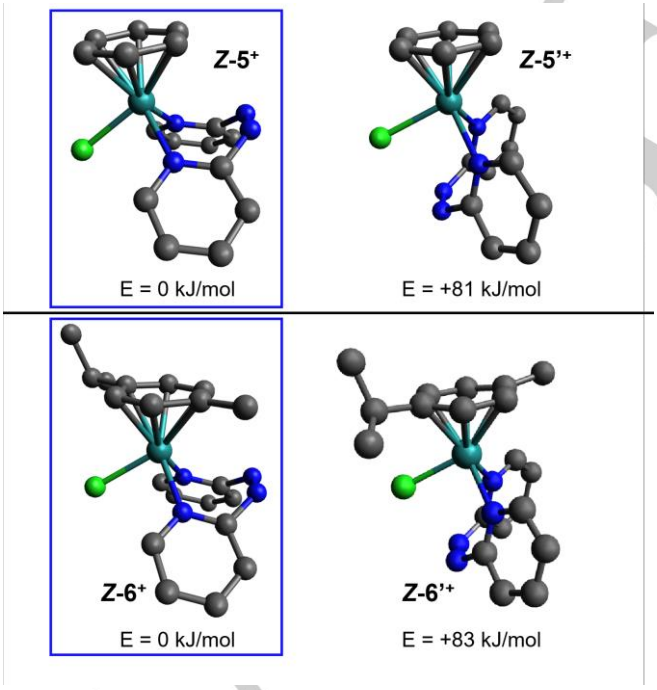

Figure 3. DFT-optimized geometries for ***Z*-5**$^+$ / ***Z*-5'**$^+$ (top) and ***Z*-6**$^+$ / ***Z*-6'**$^+$ (bottom) at the B3LYP/6-311G(d,p)/LANL2DZ level of theory. The hydrogen atoms have been removed for clarity. The structures in frame correspond to the lowest energy isomers.

Photo-induced isomerization studies

The absorption spectra of CH_2Cl_2 solutions of ***Z*-5**$^+$ and ***Z*-6**$^+$ showed a similar profile, with a sharp band at 270 nm and 276 nm, respectively and a broader one in the visible region at 424 nm and 419 nm, respectively (Figure 4).

Upon irradiation of ***Z*-5**$^+$ at 438 nm, the intensity of the band at 270 nm decreases significantly while two main bands at 363 nm and 501 nm, as well as a broader signal centered at 638 nm appear. One isosbestic point is observed at 285 nm and the resulting spectrum perfectly matches the one of ***E*-2**$^+$ (see Figure S3), thereby evidencing *Z*→*E* photo-isomerization process, as confirmed by the color change of the solution from deep green to dark red. A similar behavior was observed in the case of ***Z*-6**$^+$ with the apparition of two intense bands at 363 nm and 515 nm (four isosbestic points located at 253, 290, 424 and 439 nm) assigned to the formation of complex ***E*-3**$^+$. The clean and complete photoconversion of ***Z*-6**$^+$ into ***E*-3**$^+$ was also unambiguously confirmed by ^{1}H-NMR analysis in CD_2Cl_2, while the transformation ***Z*-5**$^+$→***E*-2**$^+$ under these conditions showed partial loss of the benzene ligand (see Figure S7,S8).

To get insight into the electronic transitions involved in ***Z*-5**$^+$ and ***Z*-6**$^+$, TD-DFT calculations were performed at the PBE0/6-311+G(d,p)/LANL2DZ level (Figure S5,S6), followed by NTO analysis of relevant vertical excitations. In the case of ***Z*-5**$^+$ and ***Z*-6**$^+$, the transitions calculated at 473 and 474 nm, respectively, close to irradiation wavelength (438 nm), revealed a change in electron density from the ruthenium center to the π* orbital of the N=N azo bond (Figure 5). This suggests that irradiation induces *Z*→*E* isomerization of the ligand, accompanied with a modification of its coordination pattern, finally leading to complexes ***E*-2**$^+$ and ***E*-3**$^+$.

A striking feature of this system is that no back photo-isomerization of ***E*-2**$^+$ or ***E*-3**$^+$ to their corresponding *Z*-complexes could be observed, whatever the wavelength of irradiation. While TD-DFT analysis reveals the occurrence of vertical excitation to the π* orbital of N=N bond at several wavelengths (Figure S9), thus possibly leading to an equilibrium between *E* and *Z* isomers upon irradiation, the higher thermodynamic stability of ***E*-2**$^+$ over ***Z*-5**$^+$ (ΔE = + 87 kJ/mol) and ***E*-3**$^+$ over ***Z*-6**$^+$ (ΔE = + 92 kJ/mol) presumably drives equilibrium towards exclusive formation of *E*-isomers (Table S1).

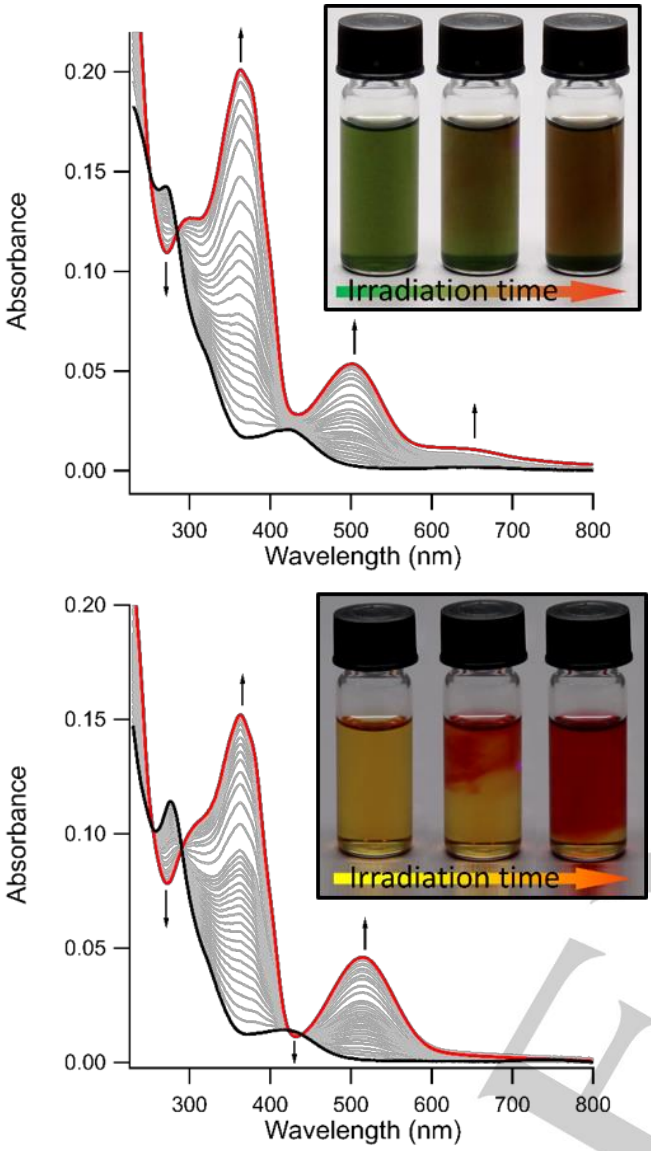

Figure 4. Absorption spectra of complexes ***Z*-5**$^+$ (top) and ***Z*-6**$^+$ (bottom) in CH_2Cl_2 (µM range concentration) at 25 °C (black line) and their stepwise evolution (step = from 1s to 30s, t_{tot} = 150s) upon irradiation at 438 nm (grey lines) with P = 12 mW/cm^2. The red line corresponds to the final state. Inset shows color evolution of irradiated solutions of ***Z*-5**$^+$ and ***Z*-6**$^+$.

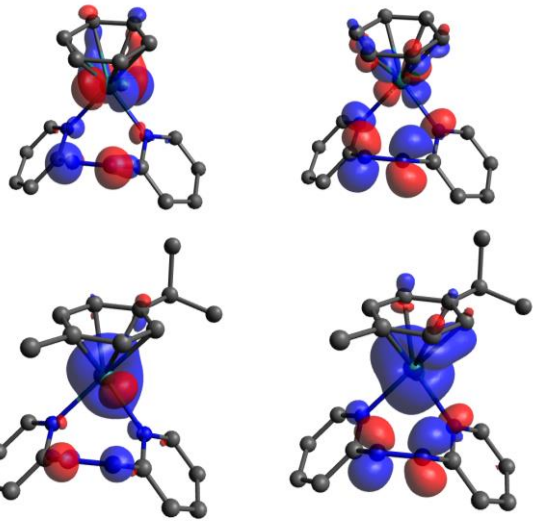

Figure 5. Relevant natural transition orbitals pairs of ***Z*-5**$^+$ (top) ***Z*-6**$^+$ (bottom) from holes (left) to particles (right) for electronic transition calculated at 473 and 474 nm respectively.

Electro-induced isomerization studies

The higher stability of the *p*-cym derivatives as compared to the bz derivatives prompted us to focus our elecrochemical investigations on ***E*-3**$^+$ and ***Z*-6**$^+$. The redox properties of the ruthenium complexes were investigated by cyclic voltammetry (CV) in CH_2Cl_2 containing tetra-*n*-butylammonium hexafluorophosphate ($TBAPF_6$, 0.2 M) as supporting electrolyte. Representative curves are shown in Figures 6,7 and S10-S12.

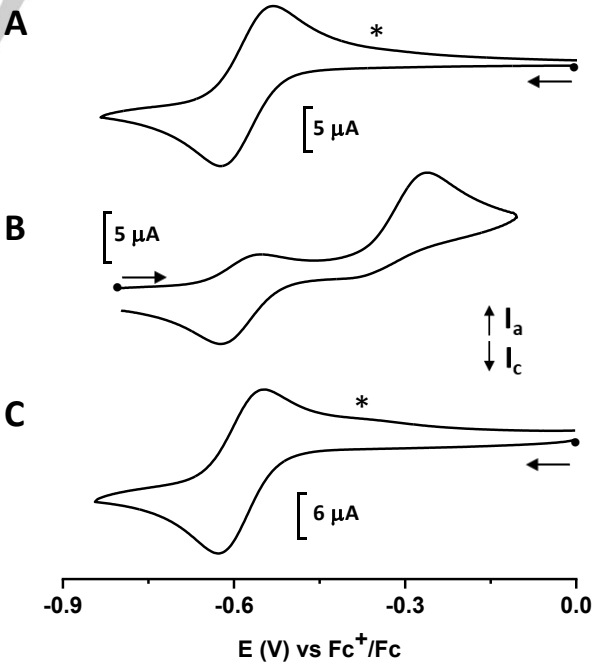

Figure 6. Cyclic voltammograms of (A) ***E*-3**$^+$, (B) ***E*-3**$^+$ after electrolysis at E_{ap} = -0.9V (1e$^-$ reduction) and (C) ***E*-3**$^+$ upon reduction at E_{ap} = -0.9V followed by reoxidation at E_{ap} = -0.2V. Scan rate 0.1 V.s^{-1}. *indicate very weak oxidation peaks.

The CV curve of ***E*-3$^+$** at a scan rate of 100 mV.s^{-1} is characterized by a reversible reduction wave at $E_{1/2}$ = -0.59 V vs Fc^+/Fc with ΔE = 75 mV (Figure 6A). By analogy with previous studies,[36] this signal is attributed to the reduction of the Ru center (Ru^{II}/Ru^{I} couple). An additional irreversible peak is also observed at E_{pc} = -1.26V (Figure S10,S11). This signal is ascribed to the reduction of the azopyridine ligand bound to the metal center, close to the reduction peak of the free ligand that is observed at E_{pc} = -1.52 V (measured under our experimental conditions).

Reduction of the ***E*-3$^+$** complex was realized by bulk electrolysis at applied potential E_{ap} = -0.9V. Under these conditions, a brown solution is obtained and coulometry measurements confirmed the monoelectronic nature of the first reduction process. The CV curves of the electrogenerated solution (Figure 6B) exhibits a non-fully reversible oxidation wave (i_{pa}/i_{pc}<1) at $E_{1/2}$ = -0.59 V attributed to the oxidation of the metal center in ***E*-3^0**. An additional irreversible peak at E_{pa} = -0.28V is also seen. Such irreversible oxidation is also observed in the voltammograms of ***E*-3$^+$** when scanning first toward low potentials (see * signal in Figure 6 and S10, weak oxidation) and its relative intensity depends on the sweep rate and on the potential of the reverse scan. These features are clearly due to the presence of chemical reactions coupled to the electron exchanges (possibly ECE processes): upon reduction of ***E*-3$^+$**, ***E*-3^0** is produced and this complex can then lead to a new more stable species (**X^0**), whose structure could not be precisely determined but in which the coordination mode around the metal center has been modified. At the CV time scale, **X^0** is barely formed whereas it is the major species obtained at the electrolysis time scale.

When the previous solution was re-oxidized by electrolysis at E_{ap} = -0.2V, the CV curve of the new solution (Figure 6C) was similar to the signal obtained for ***E*-3$^+$**, showing that the initial Ru(II) complex can be fully regenerated. These results were corroborated by UV/vis measurements (see Figure 8A): during reduction of the initial pink solution of ***E*-3$^+$**, absorption bands around 290 nm and 500 nm progressively increased, corresponding to the signature of the reduced complex. Upon re-oxidation, the initial absorption bands showing the presence of the ***E*-3$^+$** isomer were recovered. These observations are overall consistent with the transformations reported in Scheme 3a.

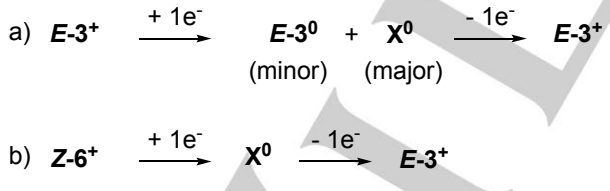

Scheme 3. Transformations of species ***E*-3$^+$** (a) and ***Z*-6$^+$** (b) upon electrolysis conditions.

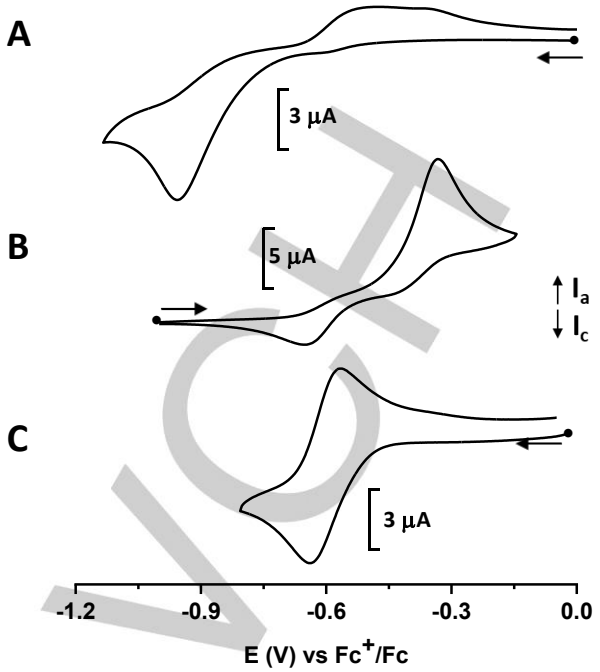

Figure 7. Cyclic voltammograms of (A) ***Z*-6$^+$**, (B) ***Z*-6$^+$** after electrolysis at E_{ap} = -1.1V (1e$^-$ reduction) and (C) ***Z*-6$^+$** upon reduction at E_{ap} = -1.1V followed by reoxidation at E_{ap} = 0V. Scan rate 0.1 V. s^{-1}.

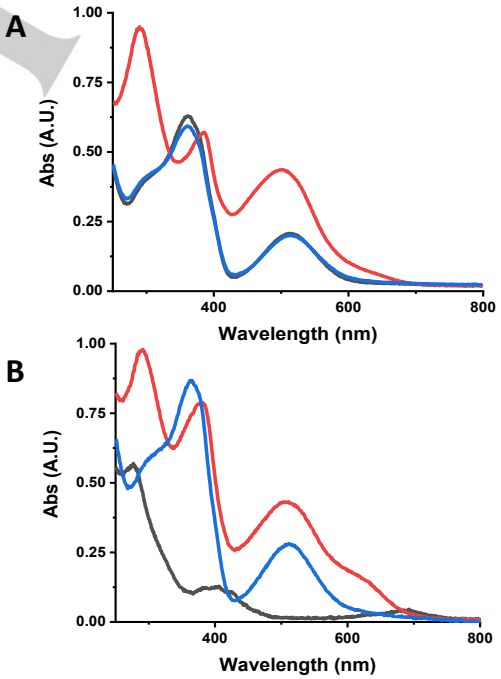

Figure 8. Spectra of (A) ***E*-3$^+$** and (B) ***Z*-6$^+$** complexes: initial solution (black line), upon 1e$^-$-reduction (red line) and upon 1e$^-$-reduction followed by 1e$^-$-oxidation (blue line).

Cyclic voltammograms of a solution of ***Z*-6$^+$** (Figure 7 and S12) display an irreversible reduction peak at -0.95V (Ru(II) → Ru(I)) and two ill-defined oxidation peaks can be seen during the return scan at -0.57V and -0.36V (reduction of the azopyridyl part is also observed at lower potential, see Figure S12). Such irreversibility of the reduction process is in accordance with

strong structural changes upon reduction of the metal center in ***Z*-6**$^+$. Upon electrolysis of this solution at E_{ap} = -1.1V (1e$^-$ per molecule, Figure 7B), a brown solution is formed and the corresponding CV curve exhibits a well-defined irreversible oxidation peak at -0.3 V coupled to a reduction peak observed during the return scan at -0.65V. This CV curve is close to the voltammogram observed after reduction of ***E*-3**$^+$, which seems to indicate that complex **X^0** is formed. Upon re-oxidation of the previous solution by electrolysis at E_{ap} = 0V (**Figure 7**C), a reversible reduction wave was seen at $E_{1/2}$ = -0.60V (ΔE_p = 80 mV). These data clearly indicate that an isomerization from ***Z*-6**$^+$ to ***E*-3**$^+$ is electrochemically triggered, by reduction of ***Z*-6**$^+$ complex followed by its re-oxidation of the solution.

These results were unambiguously confirmed by UV/Vis spectroscopy (Figure 8B): when the green initial solution of ***Z*-6**$^+$ is first reduced by bulk electrolysis (E_{app} = -1.1V), a brown solution is generated having UV-vis absorption bands close to the signal observed upon reduction of the ***E*-3**$^+$ complex, indicating that the same species **X^0** is formed when *Z* or *E* complexes are reduced. Upon re-oxidation (1e$^-$ per molecule) of the previous solution by bulk electrolysis (E_{app} = 0V), the absorption bands of the resulting pink solution clearly shows the presence of ***E*-3**$^+$ isomer, with significant bands around 360 and 510 nm. A plausible pathway for the electro-induced isomerization of ***Z*-6**$^+$ into ***E*-3**$^+$ is described in Scheme 3b.

Conclusion

A series of arene ruthenium(II) complexes derived from *E* and *Z* 2,2'-azobispyridine, among which two exhibit unprecedented coordination patterns involving the pyridine nitrogen atoms rings, was synthesized and studied. The *Z*-configured complexes were shown to undergo a complete and irreversible isomerization to their corresponding *E*-isomers (with concomitant reorganization of the coordination pattern) in response to light or electrochemical input. The generalization of such ligand behavior to other class of complexes, as well as their possible applications are currently under investigation and will be reported in due course.

Experimental Section

Equipment: Commercially available solvents and reagents were used without further purification. Absorption spectra were recorded on a Cary-4000 spectrophotometer from Agilent Technologies. Photochromic reactions were induced *in situ* by a continuous irradiation with Hg/Xe lamp (Hamamatsu, LC6 Lightningcure, 200W) equipped with a narrow band interference filter of appropriate wavelength (Semrock). The irradiation power was measured using a photodiode from Ophir (PD300-UV). Reactions were monitored by Thin Layer Chromatography (TLC) using commercial TLC Silica gel 60 F_{254} with detection by UV light (254 nm or 365 nm). Column chromatography purification was performed on CombiFlash-Rf with UV detection (two channels).

Analysis: NMR spectra were recorded using a JEOL ECS-400 spectrometer. Irradiation frequencies of ^{1}H and ^{13}C are respectively 399.78 MHz and 100.53 MHz. When specified, ^{13}C-NMR spectra of species were recorded using UDEFT sequence.[37] Chemical shifts are reported in delta (δ) units part per million (ppm) relative to the residual solvent signal or $Si(CH_3)_3$.[38,39] Coupling constants are reported in Hertz (Hz). The following abbreviations are used: s = singlet, d = doublet, t = triplet, q = quartet, sept. = septuplet, m = multiplet, br = broad. Melting points were measured with a Köfler bench previously calibrated. Infrared spectra were measured using a FTIR spectrometer from Thermo Electron Corporation with a Nexus model equipped with an ATR-Germanium module. Spectra were recorded using OMNI software. Single crystals for X-Ray diffraction were obtained as described in experimental procedures, and analyzed by the service of Structural Crystallography at Institut de Chimie des Substances Naturelles (Gif-sur-Yvette). High-resolution mass spectra (HRMS) were performed on a Bruker maXis mass spectrometer by the "Fédération de Recherche" ICOA/CBM (FR2708) platform.

Electrochemical measurements: Cyclic Voltammetry (CV) and electrolysis experiments were performed with a CH Instrument potentiostat (CHI 660B), using a standard one-compartment, three-electrode electrochemical cell. Experiments were conducted at 298 K in CH_2Cl_2 containing tetra-*n*-butylammonium hexafluorophosphate ($TBAPF_6$, 0.2M) as supporting electrolyte. Typically, millimolar solutions of the complexes were used for the electrochemical studies. The counter electrode was a platinum wire and an ALS Co. Ltd. $Ag^+|Ag$ electrode ($[Ag^+]=10^{-2}$ M in CH_3CN) was used as reference. This electrode was separated from the solution by a bridge compartment. For CV measurements, the working electrode was a 1 mm diameter platinum disk which was polished with 1 μm diamond paste before each recording. Potentials are referenced to the ferrocenium/ferrocene (Fc^+/Fc) couple, which was determined by the addition of ferrocene in the solution after each experiment. Bulk electrolyses were carried out at controlled potential with a platinum plate (~2 cm^2) as the working electrode. The auxiliary electrode was a large area platinum coil isolated from the working compartment by a glass frit containing CH_2Cl_2 + $TBAPF_6$, 0.2M. In order to monitor the evolution of the species during bulk electrolysis, a UV/Vis probe (1 mm all–quartz Helmma immersion probe) connected to the spectrophotometer (Varian Cary 60) through an optical fiber was dipped in the solution. Spectroelectrochemical experiments were also conducted using a UV-vis cell (1 mm) equipped with an Ag wire (pseudo reference electrode), a Pt wire (counter electrode) and a platinum grid (working electrode), the cell being inserted in the UV/vis spectrometer. All measurements were taken in absence of oxygen, by bubbling argon before experiments.

Molecular modeling: Molecular geometries were optimized by the DFT method using the B3LYP functional, the 6-311G(d,p) basis set and LANL2DZ for the ruthenium, as implemented in the Gaussian09 software package.[40] Results were viewed with Avogadro 1.1.1[41] software and the absence of negative frequency was checked to confirm the obtention of an energy minimum. Oscillator strengths were calculated by TDDFT method using PBE0 functional, the 6-311+G(d,p) basis set[42] and LANL2DZ for the ruthenium.

General procedure for the determination of molar absorption coefficient: Around 1.00 mg of the compound is precisely weighted and dissolved in 6 mL of solvent to give a S_0 solution. Eight solutions were prepared at different concentrations by adding 20, 50, 100, 200, 300 ,400, 500 or 600 µL of S_0 to 2.5 mL of solvent. The spectrum of each solution was recorded and the absorbance corresponding to a local maximum was plotted as a function of concentration. The resulting data were then linearized according to Beer-Lambert law.

***trans*-2,2'-azobispyridine *E*-1**[34]**:** To an ice-cold solution of bleach (4.8% NaOCl, 150 mL, 54.0 mmol, 5.0 eq.) was added dropwise a solution of 2-aminopyridine (1.00 g, 10.6 mmol, 1.0 eq.) in water (10 mL). After stirring at rt for 1 h, the reaction mixture was extracted with CH_2Cl_2 (*ca.* 3×150 mL), the organic layer was dried over $MgSO_4$, filtered and the solvent removed under reduced pressure. Purification by silica gel chromatography (PE/EA: 5/5 to 3/7) afforded ***E*-1** (448 mg, 2.44 mmol, 46%). Red solid; Rf: 0.26 (EA); ^{1}H NMR (400 MHz, $CDCl_3$): δ ppm 8.71 (d, *J* = 5.2 Hz, 2H), 7.99 (d, *J* = 1.6 Hz, 2H), 7.50 (dd, *J* = 5.2, 1.6 Hz, 2H); ^{13}C NMR (100 MHz, $CDCl_3$): δ ppm 163.3, 150.5, 146.5, 126.5, 114.9.

***cis*-2,2'-azobispyridine *Z*-1:** A solution of ***E*-1** (353 mg, 1.90 mmol, 1.0 eq.) in CH_2Cl_2 (50 mL) was irradiated for 4 h at 315 nm. The reaction mixture was concentrated under reduced pressure and the *E* and *Z* isomers were separated by silica gel chromatography in the dark (PE/EA: 6/4 to 4/6) to afford the starting material ***E*-1** (210 mg, 1.14 mmol, 59%) and ***Z*-1** (144 mg, 0.779 mmol, 41%). The latter can be used within a few days when stored in the dark at –20°C. Orange solid; Rf: 0.61 (PE/EA: 2/8) ^{1}H NMR (400 MHz, $CDCl_3$): δ ppm 8.01 (d, *J* = 5.6 Hz, 2H), 7.56 (d, *J* = 2.0 Hz, 2H), 7.09 (dd, *J* = 5.6, 2.0 Hz, 2H); ^{13}C NMR (100 MHz, ($CDCl_3$): δ ppm 164.9, 148.5, 145.9, 123.2, 119.9.

General procedure for the synthesis of [Ru(Ar)(azpy)Cl]PF_6 synthesis: To a solution of $[Ru(Ar)Cl_2]_2$ (0.08 mmol, 0.5 eq.) in MeOH (5 mL) under argon was added dropwise a solution of **1** (30 mg, 0.16 mmol, 1.0 eq.) in MeOH (1.5 mL). After stirring at rt for 30 min, NH_4PF_6 (132 mg, 0.80 mmol, 5.0 eq.) was added and the mixture was stirred for 10 min. The precipitate was filtered and washed with Et_2O to afford **[Ru(Ar)(azpy)Cl]PF_6.**

[Ru(bz)(*trans*-azpy)Cl]PF_6 *E*-2$^+$: 92% yield, black red solid; Rf: 0.29 (CH_2Cl_2/MeOH: 95/5); m.p. > 270°C; ^{1}H NMR (400 MHz, CD_2Cl_2): δ ppm 9.48 (d, *J* = 5.6 Hz, 1H), 8.90 (d, *J* = 4.0 Hz, 1H), 8.73 (d, *J* = 7.6 Hz, 1H), 8.35 (td, *J* = 7.6, 1.2 Hz, 1H), 8.14-8.05 (m, 2H), 7.86 (m, 1H), 7.79-7.75 (m, 1H), 6.32 (s, 6H); ^{13}C UDEFT NMR (100 MHz, CD_2Cl_2): δ ppm 155.0, 149.6, 141.6, 139.8, 131.3, 130.0, 129.5, 116.4, 91.7, 2Cq not visible; IR (ATR): 2986; 1467; 1439; 1390; 1239; 1154; 1050; 963; 835; 799; 744 cm^{-1}; ε (λ= 363 nm, MeOH): 10 965 L·mol^{-1}·cm^{-1}; HRMS (ESI) m/z: Calcd for $C_{16}H_{14}ClN_4Ru^+$ [M]$^+$: 398.9945, found 398.9952.

[Ru(*p*-cym)(*trans*-azpy)Cl]PF_6 *E*-3$^+$[35]: 71% yield, black red solid; Rf: 0.23 (CH_2Cl_2/MeOH: 95/5); m.p. 182°C; ^{1}H NMR (400 MHz, CD_2Cl_2): δ ppm 9.48 (dd, *J* = 5.6, 1.2 Hz, 1H), 8.89 (dt, *J* = 4.4, 0.8 Hz, 1H), 8.72 (dd, *J* = 7.6, 0.8 Hz, 1H), 8.33 (td, *J* = 8.0, 1.6 Hz, 1H), 8.11-8.05 (m, 2H), 7.89 (td, *J* = 6.0, 1.6 Hz, 1H), 7.77 (m, 1H), 6.38 (d, *J* = 6.8 Hz, 1H), 6.33 (d, *J* = 6.8 Hz, 1H), 6.04 (d, *J* = 6.4 Hz, 2H), 2.57 (sept., *J* = 6.8 Hz, 1H), 2.27 (s, 3H), 0.99 (t, *J* = 6.8 Hz, 6H); ^{13}C NMR (100 MHz, CD_2Cl_2): δ ppm 163.0, 162.4, 154.2, 148.8, 140.6, 139.0, 130.0, 129.3, 128.4, 115.7, 111.1, 110.1, 92.0, 90.7, 88.4, 87.6, 31.0, 21.5, 21.4, 18.9; IR (ATR): 2973; 2899; 1466; 1436; 1375; 1248; 1054; 963; 834; 794; 744; 694 cm^{-1}; ε (λ= 363 nm, MeOH): 13 368 L·mol^{-1}·cm^{-1}; HRMS (ESI) m/z: Calcd for $C_{20}H_{22}ClN_4Ru^+$ [M]$^+$: 455.0576, found 455.0577.

[Ru(hmbz)(*trans*-azpy)Cl]PF_6 *E*-4$^+$: 86% yield, black red solid; Rf: 0.26 (CH_2Cl_2/MeOH: 95/5); m.p. > 270°C; ^{1}H NMR (400 MHz, CD_2Cl_2): δ ppm 8.82 (dd, *J* = 6.0, 1.2 Hz, 1H), 8.78 (dd, *J* = 4.0, 0.8 Hz, 1H), 8.71 (dd, *J* = 8.0, 0.8 Hz, 1H), 8.31 (td, *J* = 8.0, 1.6 Hz, 1H), 8.12 (td, *J* = 8.0, 2.0 Hz, 1H), 8.01-7.98 (m, 1H), 7.96-7.91 (m, 1H), 7.73-7.68 (m, 1H), 2.01 (s, 18H); ^{13}C UDEFT NMR (100 MHz, CD_2Cl_2): δ ppm 164.4, 151.2, 149.6, 141.2, 139.9, 129.8, 129.4, 128.0, 118.2, 103.4, 16.1, 1Cq not visible; IR (ATR): 2985; 2892; 1457; 1432; 1367; 1243; 1072; 899; 836; 780; 741; 699; 679 cm^{-1}; ε (λ= 317 nm, MeOH): 6 832 L·mol^{-1}·cm^{-1}; HRMS (ESI) m/z: Calcd for $C_{22}H_{26}ClN_4Ru^+$ [M]$^+$: 483.0889, found 483.0889.

[Ru(bz)(*cis*-azpy)Cl]PF_6 *Z*-5$^+$: 89% yield, dark green solid; Rf: 0.37 (CH_2Cl_2/MeOH: 95/5); ^{1}H NMR (400 MHz, CD_2Cl_2): δ ppm 9.04 (d, *J* = 5.2 Hz, 2H), 8.08 (td, *J* = 7.6, 1.2 Hz, 2H), 7.57 (d, *J* = 7.6 Hz, 2H), 7.41 (m, 2H), 5.91 (s, 6H); ^{13}C UDEFT NMR (100 MHz, CD_2Cl_2): δ ppm 163.6, 154.4, 142.3, 125.9, 119.8, 86.7; IR (ATR): 1598; 1441; 833; 784; 741 cm^{-1}.

[Ru(*p*-cym)(*cis*-azpy)Cl]PF_6 *Z*-6$^+$: 82% yield, yellow solid; Rf: 0.23 (CH_2Cl_2/MeOH: 95/5); ^{1}H NMR (400 MHz, CD_2Cl_2): δ ppm 8.98 (d, *J* = 5.6 Hz, 2H), 8.09 (td, *J* = 8.0, 1.2 Hz, 2H), 7.60 (d, *J* = 7.6 Hz, 2H), 7.42 (td, *J* = 6.4, 0.8 Hz, 2H), 5.74 (d, *J* = 6.0 Hz, 2H), 5.58 (d, *J* = 6.0 Hz, 2H), 2.66 (sept., *J* = 6.8 Hz, 1H), 2.04 (s, 3H), 1.22 (d, *J* = 6.8 Hz, 6H); ^{13}C UDEFT NMR (100 MHz, CD_2Cl_2): δ ppm 163.8, 153.5, 142.3, 126.1, 119.9, 106.6, 101.3, 85.3, 84.5, 31.4, 22.3, 18.8; IR (ATR): 2971; 1598; 1466; 1429; 1058; 1026; 836; 783; 762 cm^{-1}.

Acknowledgements

We thank Nolwenn Mahieu and Sylvain Badin for preliminary synthesis of Ru-complexes, Dr. Stéphane Maisonneuve for assistance with NMR measurements and ENS Paris-Saclay for an international incoming mobility fellowship to DK. This work was performed using HPC resources from the "Mésocentre" computing center of CentraleSupélec and École Normale Supérieure Paris-Saclay supported by CNRS and Région Île-de-France (http://mesocentre.centralesupelec.fr/).

Keywords: azobispyridine • arene ruthenium • photochemistry • electrochemistry • coordination pattern

Entry for the Table of Contents

Insert graphic for Table of Contents here.

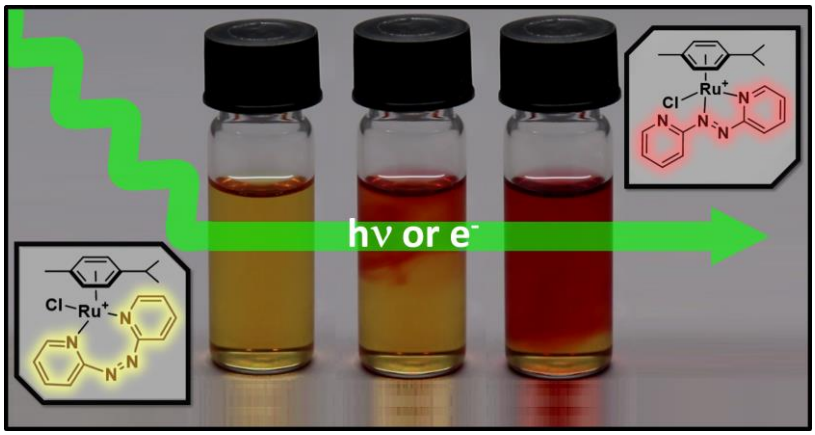

One shot switch in response to light or electrochemical stimuli of 2,2'-azobispyridine involved in a 7-membered chelate ring with a Ru(II) metal center is disclosed. The molecular pathways at work in the course of this transformation were investigated by a combination of analytical and computational techniques, thereby providing a rational for the efficient and irreversible nature of the process.

Institute and/or researcher Twitter usernames: ((optional))

[1] A. Bianchi, E. Delgado-Pinar, E. García-España, C. Giorgi, F. Pina, *Coord. Chem. Rev.* **2014**, *260*, 156–215.
[2] M. Dommaschk, M. Peters, F. Gutzeit, C. Schütt, C. Näther, F. D. Sönnichsen, S. Tiwari, C. Riedel, S. Boretius, R. Herges, *J. Am. Chem. Soc.* **2015**, *137*, 7552–7555.
[3] S. J. Dougan, M. Melchart, A. Habtemariam, S. Parsons, P. J. Sadler, *Inorg. Chem.* **2006**, *45*, 10882–10894.
[4] A. H. Velders, H. Kooijman, A. L. Spek, J. G. Haasnoot, D. de Vos, J. Reedijk, *Inorg. Chem.* **2000**, *39*, 2966–2967.
[5] A. C. G. Hotze, M. Bacac, A. H. Velders, B. A. J. Jansen, H. Kooijman, A. L. Spek, J. G. Haasnoot, J. Reedijk, *J. Med. Chem.***2003**, *46*, 1743–1750.
[6] K. Aoki, M. Nakagawa, K. Ichimura, *J. Am. Chem. Soc.* **2000**, *122*, 10997–11004.
[7] L. Lin, Z. Yan, J. Gu, Y. Zhang, Z. Feng, Y. Yu, *Macromol. Rapid Commun.* **2009**, *30*, 1089–1093.
[8] K. Han, W. Su, M. Zhong, Q. Yan, Y. Luo, Q. Zhang, Y. Li, *Macromol. Rapid Commun.* **2008**, *29*, 1866–1870.
[9] V. Balzani, A. Credi, M. Venturi in Molecular Devices and Machines: Concepts and Perspectives for the Nanoworld, Second Edition, Wiley-VCH, **2008**.
[10] H. Ren, P. Yang, F. M. Winnik, *Polym. Chem.* **2020**, *11*, 5955–5961.
[11] F. Haque, A. Halder, S. Ghosh, D. Ghoshal, *Polyhedron* **2019**, *161*, 289–297.
[12] M.-X. Li, X.-Q. Wang, Z.-X. Wang, M. Shao, S. Zhu, X. He, *Inorg. Chim. Acta* **2016**, *446*, 143–149.
[13] P. Rajakannu, R. Howlader, A. C. Kalita, R. J. Butcher, R. Murugavel, *Inorg. Chem. Front.* **2015**, *2*, 55–66.
[14] D. K. Maity, A. Dey, S. Ghosh, A. Halder, P. P. Ray, D. Ghoshal, *Inorg. Chem.* **2018**, *57*, 251–263.
[15] F. Arslan Biçer, S. Yildirim, W. Kaim, M. Bubrin, *J. Coord. Chem.* **2017**, *70*, 2853–2869.
[16] F. Arslan, H. Ölmez, M. Odabaşoğlu, O. Büyükgüngör, *Z. Anorg. Allg. Chem.* **2010**, *636*, 1641–1644.
[17] N. E. Clayman, M. A. Manumpil, B. D. Matson, S. Wang, A. H. Slavney, R. Sarangi, H. I. Karunadasa, R. M. Waymouth, *Inorg. Chem.* **2019**, *58*, 10856–10860.
[18] S. Maity, S. Kundu, T. Weyhermüller, P. Ghosh, *Inorg. Chem.* **2015**, *54*, 1300–1313.
[19] G. Pourrieux, F. Fagalde, I. Romero, X. Fontrodona, T. Parella, N. E. Katz, *Inorg. Chem.* **2010**, *49*, 4084–4091.
[20] V. W.-W. Yam, V. C.-Y. Lau, L.-X. Wu, *J. Chem. Soc., Dalton Trans.* **1998**, 1461–1468.
[21] S. Sengupta, I. Chakraborty, A. Chakravorty, *Eur. J. Inorg. Chem.* **2003**, *6*, 1157–1160.
[22] B. Santra, *ChemistrySelect* **2019**, *4*, 1866–1871.
[23] Y. Karaman, N. Menek, F. A. Bicer, H. Olmez, *Int. J. Electrochem. Sci.* **2015**, *10*, 3106–3116.
[24] Q.-X. Zhou, Y. Zheng, T.-J. Wang, Y.-J. Chen, K. Li, Y.-Y. Zhang, C. Li, Y.-J. Hou, X.-S. Wang, *Chem. Commun.* **2015**, *51*, 10684–10686.
[25] S. Goswami, R. N. Mukherjee, A. Chakravorty, *Inorg. Chem.* ,**1983**, *22*, 2825–2832.
[26] M. Bardají, M. Barrio, P. Espinet, *Dalton Trans.* **2011**, *40*, 2570–2577.
[27] S. Kulovi, S. Dalbera, S. K. Dey, S. Maiti Choudhury, H. Puschmann, E. Zangrando, S. Dalai, *ChemistrySelect* **2018**, *3*, 5233–5242.
[28] A. Dogan, B. Sarkar, A. Klein, F. Lissner, T. Schleid, J. Fiedler, S. Záliš, V. K. Jain, W. Kaim, *Inorg. Chem.* **2004**, *43*, 5973–5980.
[29] W.-Y. Wong, S.-H. Cheung, S.-M. Lee, S.-Y. Leung, *J. Organomet. Chem.* **2000**, *596*, 36–45.
[30] O. Theilmann, W. Saak, D. Haase, R. Beckhaus, *Organometallics* **2009**, *28*, 2799–2807.
[31] H. Tsurugi, H. Tanahashi, H. Nishiyama, W. Fegler, T. Saito, A. Sauer, J. Okuda, K. Mashima, *J. Am. Chem. Soc.* **2013**, *135*, 5986–5989.
[32] M. Camalli, F.Caruso, G.Mattogno, E. Rivarola, *Inorg. Chim. Acta* **1990**, *170*, 225–231.
[33] D. A. Baldwin, A. B. P. Lever, R. V. Parish, *Inorg. Chem.* **1969**, *8*, 107–115.
[34] N. Campbell, A. W. Henderson, D. Taylor, *J. Chem. Soc.*, **1953**, 1281–1285.
[35] A. Das, T. M. Scherer, A. D. Chowdhury, S. M. Mobin, W. Kaim, G. K. Lahiri, *Inorg. Chem.* **2012**, *51*, 1675–1684.
[36] J. Otsuki, K. Sato, M. Tsujino, N. Okuda, K. Araki, M. Seno, *Chem. Lett.* **1996**, *25*, 847–848.
[37] M. Piotto, M. Bourdonneau, K. Elbayed, J.-M. Wieruszeski, G. Lippens, *Magn. Reson. Chem.* **2006**, *44*, 943–947.
[38] H. E. Gottlieb, V. Kotlyar, A. Nudelman, *J. Org. Chem.* **1997**, *62*, 7512–7515.
[39] G. R. Fulmer, A. J. M. Miller, N. H. Sherden, H. E. Gottlieb, A. Nudelman, B. M. Stoltz, J. E. Bercaw, K. I. Goldberg, *Organometallics* **2010**, *29*, 2176–2179.
[40] Gaussian 09, Revision E.01, M. J. Frisch, G. W. Trucks, H. B. Schlegel, G. E. Scuseria, M. A. Robb, J. R. Cheeseman, G. Scalmani, V. Barone, B. Mennuci, G. A. Petersson *et al*., Gaussian Inc., Wallingford CT, **2009**.
[41] M. D. Hanwell, D. E. Curtis, D. C. Lonie, T. Vandermeersch, E. Zurek, G. R. Hutchison, *J. Cheminform.* **2012**, *4*, 1–17.
[42] D. Jacquemin, E. A. Perpète, G. E. Scuseria, I. Ciofini, C. Adamo, *Chem. Phys. Lett.* **2008**, *465*, 226–229.